Sputtering yields of compounds using argon ions

M P Seah, T S Nunney

Sputtering yields of compounds using argon ions

M P Seah[1] and T S Nunney[2]

[1]Analytical Science Division, National Physical Laboratory, Teddington, Middlesex TW11 0LW, UK,
[2]Thermo Fisher Scientific, The Birches Industrial Estate, Imberhorne Lane, East Grinstead, West Sussex RH19 1UB, UK

emails: martin.seah@npl.co.uk and tim.nunney@thermofisher.com

Abstract. An analysis is made of published sputtering yield data for compounds using argon primary ions at normal incidence to evaluate the validity of simple predictive equations. These are sputtering yields at dynamical equilibrium. First, two archetypal compounds are analysed: GaAs with constituent elements of similar atomic number and weak preferential sputtering, and Ta_2O_5 with constituent elements of widely separate atomic number and strong preferential sputtering. The agreements of the sputtering yields predicted by the semi-empirical linear cascade theory are excellent when the appropriate parameters are interpolated, rather than using an average atomic number. The effect of preferential sputtering is included within the framework of the simple pair-bond theory. The average ratios of the data to the initial predictions for GaAs and Ta_2O_5 are 1.01 ± 0.06 and 1.00 ± 0.07, respectively. Extension of this analysis to a range of oxides shows that the heat of reaction of the oxidation process needs inclusion. It is here that the effect of preferential sputtering can lead to an expansion of the uncertainties. SiO_2 is often used as a reference material and so the published yield data are analysed in detail. These show an extremely broad scatter and so new experimental data are measured. These new results are in the upper range of previous data and correlate with the semi-empirical theory with a scatter of only 9%. These correlations show that the semi-empirical linear cascade theory is excellent for predicting the energy dependence of the yield and can be excellent for absolute yields where the compound heat of formation is low.

Keywords: Argon ions, GaAs, SiO_2, Sputtering yields, Ta_2O_5

PACS:34.35.+a; 68.49.Sf; 68.55.jd; 79.20.Rf; 79.60.Dp; 81.70.Jb.

Submitted to Journal of Physics D

I. Introduction

The sputtering of materials using inert gas primary ions, particularly argon, is a routine part of surface and thin film analysis for compositional depth profiling using Auger electron spectroscopy (AES) or X-ray photoelectron spectroscopy (XPS) [1,2]. Other inert gases are also used to improve the depth resolution, or to ensure that spectral peaks from the inert gas are well separated from the spectral peaks required to identify the materials being profiled, or to reduce the effects of preferential sputtering. Nevertheless, argon is still the ion of first choice for compositional depth profiling using AES or XPS by most analysts.

Recently, we have analysed extensive data for the sputtering yields of elemental solids in order to develop the semi-empirical theory of sputtering yields for bombardment by argon [3], neon, and xenon [4,5]. That theory provides a very good description to the absolute yields for the energy range 250 to 10000 eV and, for the elemental solids analysed, the scatter between the prediction at normal incidence and the experimental data for Ar^+ is 9%. A figure of 9% is better than the current laboratory-to-laboratory reproducibility of sputtering yield measurements. Similar scatters are

obtained between the predictions of the semi-empirical model and the data for Ne^+ and Xe^+. This theory is based on the approach of Matsunami *et al.* [6] which is based, in turn, on the linear cascade theory of Sigmund [7]. Two extra terms were included that describe, using known materials parameters, the arbitrary *Q* factors that scale the yield in Matsunami *et al*'s approach. The above correlation was for normally incident ions and, in reference [3], the scaling for 45°, based on the work of Yamamura *et al.* [8], is given together with new data for a range of elements at 45° incidence confirming the predictive value of the semi-empirical theory.

In practice, much of compositional depth profile analysis is of compounds and not for elemental layers but the extent of basic experimental and theoretical work for compounds is small. In this study, we consider the absolute sputtering yields of compounds and the extent to which the popular linear cascade approach is valid.

Part of the need for the above semi-empiricism is that the basic theory is not yet at the level of completion to generate the required accuracy. More importantly, the effects of damage by the impacting ions, and the inclusion of inert gas atoms [4] that occur in sputter depth profiles, are extremely difficult to compute in a generic manner. The development of damage will increase the sputtering yield but the removal of energy by the need to sputter any implanted inert gas atoms will then reduce that yield; albeit not to the same extent. These effects, which are difficult to include in the basic theory, are automatically included within the *Q* parameter in the semi-empirical approach, since this is based on experimental data that include such effects. Of course, for sputter depth profiling, it is this sputtering yield at dynamical equilibrium with the damage and primary ion implantation that is required rather than the sputtering yield for the original material.

Modern molecular dynamics approaches to determining sputtering yields include significantly more physics than the above semi-empirical approach. However, these methods, whilst providing splendid visualisation of the sputtering process, often do not predict absolute sputtering yields that correlate with experimental data. Any lack of fit may or may not be significant. It may be that, sometimes, there is a simple, undiscovered scaling effect or it may be that the underlying mechanism proposed is, in some way, basically invalid. Molecular dynamics methods importantly allow the study of sputtering for arbitrarily shaped surfaces and for nanoparticles, difficult to analyse with the semi-empirical theory. Thus, for instance, Zimmermann and Urbassek [9] calculate the sputtering yields of 20 nm gold nanoparticles by Au primary ions, to be 489 to 793 at 16 keV and 2955 at 64 keV, during the first 40 ps from impact. The same calculations lead to sputtering yields of 298 and 616 for planar surfaces at these two energies which they note are high when compared with the experimental yield of ~30 for 16 keV Xe sputtering Au [10]. With some uncertainty in the data, some uncertainty arising from the use of Xe primary ions instead of Au, the overall difference may or may not be significant. Using the semi-empirical theory, Seah [11] showed that for gold using 16 and 64 keV Au primary ions, the predicted yields were 13 and 20 but that, if the theory were extended to include the thermal spike approach of Sigmund and Claussen [12], the values increased to 17 and 40, respectively. Seah's [11] full calculations described the experimental data of Bouneau *et al.* [13] with a standard deviation of 17% for primary ion energies up to 2800 keV, with primary ion clusters up to Au_{13}^+ and yields up to 14313. It is clear that the molecular dynamics simulations, at least for the flat surface, were generating yields that were a factor of 16 ± 3 times too high compared with those at equilibrium and so may also be too high in nanoparticles. It is not clear if this is a simple scaling issue but the rather large cluster sizes of the secondary particles generated in the simulations do not appear in SIMS spectra with equivalent intensities. On the other hand, the molecular dynamics approach of Samela *et al*. [14] gives results over the wide energy range from 100 to 40000 eV with a factor of only 1.3 above the experimental data. At the present time, molecular dynamics simulations are for the first ion into the sample, giving the static sputtering yield, and do not consider the evolution of the dynamical equilibrium composition that gives the dynamic sputtering yield needed for measurements in compositional depth profiling.

In the above work, which is for elemental samples, the issue of preferential sputtering was not relevant. However, many practical profiles also include compounds that are III-V or II-VI semi-conductors or oxides and, for these, preferential sputtering will occur. The reasons for preferential sputtering are many but the result is that the outermost monolayer may have one composition and under this layer will be a region with another average composition that generally differs from the bulk composition. Even if one could start with a clean stoichiometric sample, this preferential sputtering is

well established after removing a few monolayers, although full equilibrium of the altered region may require significantly more sputtering. After further sputtering, physical structures may appear with their own unique compositions [15]. These will not be considered here. The preferential sputtering and altered layer are thought to affect the sputtering yield. If the preferential sputtering and altered layer change with the primary ion beam energy, then the energy dependence of the sputtering yield may also be affected. Analysts often use lower beam energies to reduce the preferential sputtering although the evidence to support this is unclear. Lower beam energies will reduce the altered layer thickness and, for an instrument under good control, will generally improve the depth resolution.

In the present work, the effectiveness of the semi-empirical theory to predict the absolute dynamic sputtering yield, and also its energy dependence, is evaluated for application to the argon sputtering of compounds at normal incidence. This is tested using published data for GaAs, Ta_2O_5 and SiO_2 over a range of energies, and for a range of oxides at a few energies. GaAs and Ta_2O_5 are archetypal systems for which extensive data exist; one being a semi-conductor with elements of close atomic number and the other an oxide with elements widely spaced in atomic number. SiO_2 is included since it is often profiled and is used as a reference material. However, the published data are very scattered and so new experimental data are acquired here. The only other compound with extensive data is InP but significant decomposition means that this system requires more extensive analysis.

2. The Semi-empirical approach

2.1. Sputtering yields for elements

At normal incidence, the generalized development [3,6] of Sigmund's theory [7] gives the sputtering yield, *Y*, as

$$Y = \frac{C\ Q}{U_o}\ \frac{\alpha\, S_n(E)}{1+A s_e(\varepsilon)}\ \left(1-\left(\frac{E_{th}}{E}\right)^{1/2}\right)^{2.8} \qquad (1)$$

where $S_n(E)$ is the nuclear stopping cross section per atom and U_o the surface binding energy per atom. The heat of sublimation per atom sputtered is often equated to U_o and new calculations for this parameter have been provided [3]. The coefficient C is generally given as 0.042 Å^{-2} with U_o expressed in eV per atom.

Here, the nuclear stopping cross section is given by [16]

$$S_n(E) = 4\pi Z_1 Z_2\ \frac{e_o^2}{4\pi\varepsilon_o}\ a_{12}\ \frac{M_1}{M_1+M_2}\ s_n(\varepsilon) \qquad (2)$$

where Z_1 and M_1 are the atomic number and mass of the primary ion and Z_2 and M_2 are similarly for the target atoms, e_o is the electronic charge and ε_o is the permittivity of vacuum. The parameter a_{12} is given by

$$a_{12} = \left(\frac{9\pi^2}{128}\right)^{1/3}\ \frac{a_o}{(Z_1^{2/3}+Z_2^{2/3})^{1/2}} \qquad (3)$$

where a_o is the Bohr radius of 0.529 Å and, as derived by Matsunami *et al.* [17] for Lindhard, Scharff and Schiott's theory [16],

$$s_n(\varepsilon) = \frac{3.441\ \varepsilon^{1/2}\ \ln(\varepsilon+2.718)}{1+6.355\ \varepsilon^{1/2}+\varepsilon(6.882\varepsilon^{1/2}-1.708)} \qquad (4)$$

Evaluation of the coefficients in equation (2) gives

$$S_n(E) = \frac{84.78\ Z_1 Z_2}{(Z_1^{2/3} + Z_2^{2/3})^{1/2}} \frac{M_1}{M_1 + M_2} s_n(\varepsilon) \qquad \text{eV Å}^2 \text{ / atom} \tag{5}$$

and, if E is in eV,

$$\varepsilon = \frac{0.03255}{Z_1 Z_2 (Z_1^{2/3} + Z_2^{2/3})^{1/2}} \frac{M_2}{M_1 + M_2} E \tag{6}$$

In equation (1), $s_e(\varepsilon)$ is the inelastic, electronic stopping power where

$$s_e(\varepsilon) = k\varepsilon^{1/2} \tag{7}$$

and [16]

$$k = G^{1/2} \frac{(M_1 + M_2)^{3/2}}{M_1^{3/2} M_2^{1/2}} \frac{Z_1^{2/3} Z_2^{1/2}}{(Z_1^{2/3} + Z_2^{2/3})^{3/4}} \tag{8}$$

where G = 0.00629 u (u represents the unified atomic mass unit). In Matsunami *et al*'s formulation [6]

$$A = D U_o \tag{9}$$

with D = 0.35 eV^{-1}. Fitting then gave

$$\alpha = 0.08 + 0.164(M_2 / M_1)^{0.4} + 0.0145(M_2 / M_1)^{1.29} \tag{10}$$

with

$$E_{th} / U_o = 1.9 + 3.8(M_1 / M_2) + 0.134(M_2 / M_1)^{1.24} \tag{11}$$

In reference [4], an analytical form is derived for Matsunami *et al*'s [6] scaling constants, Q for each element. For argon primary ions:

$$Qr^3 = g^3 \left\{ \exp\left[-\frac{(M_2 - b)^2}{2c^2} \right] \right\} + h^3 \left\{ 1 - \exp\left[-\frac{(M_2 - d)^2}{f^2} \right] \right\} \tag{12}$$

where b = 15.483 u, c = 19.83 u, d = 16 u, f = 50 u, g = 0.274 nm and h = 0.281 nm. The average interatomic spacing, r, is given by

$$r^3 = \frac{M_2}{1000 \rho N} \tag{13}$$

The r^3 term is the most significant part of Q and is part of Sigmund's theory [7]. Equation (12) provides Q values for all elements rather than using a look-up table based on measured data for each of a limited range of elements. The target density ρ is in kg m^{-3} and N is Avogodro's number.

These equations provide sputtering yields for elements and, for sputtering by Ne^+, Ar^+ and Xe^+, an average overall scatter of 12% was obtained [4]. For Ne^+ and Xe^+ a more generic form of equation (12) is used.

2.2. Sputtering yields for compounds

For compounds, a simple intuitive stopping power would be a linear combination of the elemental stopping powers scaled by the respective atomic fractions, i.e. Bragg's rule [18]. Sigmund [19] notes that this has limited accuracy particularly when M_1 is intermediate between two widely different compound masses M_{2A} and M_{2B}. Similarly, Malherbe [20], in his thorough and extensive review of compound semiconductor sputtering yields, tests a wide range of equations, although not Matsunami *et al*'s [6], and suggests computing with the target effectively "elemental" with an average atomic number, $Z_2 = X_A Z_{2A} + X_B Z_{2B}$ where X_A is the atomic fraction of A in the compound of A and B, etc. The effective atomic mass, M_2, is derived similarly but Malherbe notes that semiconductors such as InP, with widely different masses, would not be a favourable case for this approach. Indeed, InP rapidly develops an interesting surface structure with In regions that grossly change the nature of the surface and hence the yield [15]. Such aspects are beyond normal calculations for sputtering yields.

In the present work, when computing sputtering yields for compounds, the values of the main parameters in equation (1) are interpolated from the values for the separate elements to find an effective value. The parameters interpolated are Qr^3, α, $S_n(E)$, E_{th} and k from equations (12), (10), (5), (11), and (8) but the average interatomic spacing, r, is evaluated from the bulk density of the compound, unless otherwise stated. U_o is discussed below. By interpolation, for instance, $Q_{2A} r_{2A}^3$ and $Q_{2B} r_{2B}^3$ for M_{2A} and M_{2B} are calculated from equation (12) and then Qr^3 is taken as $X_A (Q_{2A} r_{2A}^3) + X_B (Q_{2B} r_{2B}^3)$ rather than directly from equation (12) for the average value of M_2. Thus, for instance, the stopping power is the average stopping power of the constituents rather than the stopping power for a sample of average atomic number and mass. For any effect that is a linear function of M or Z, the difference would be zero, but in many of the cases studied here, this is not the case.

In the computer program SRIM, the stopping of more than 150 compounds is evaluated and suitable corrections can be applied for the bonding states [21]. This significantly improves accuracy over the use of Bragg's rule, which ignores changes due to chemical bonding. The bonding corrections range up to 20% and are essential for accurate stopping and range calculations where an accuracy of 4% is achieved. However, in the highly damaged region from which sputtering occurs, the bulk bonding may or may not be appropriate.

Two other equations feature significantly in reviews of this area. The first concerns the composition of the surface altered layer at equilibrium sputtering, with or without Gibbsian segregation [22], X_A^S and X_B^S

$$\frac{X_A^S}{X_B^S} = \frac{X_A}{X_B} \frac{Y_B^S}{Y_A^S} \tag{14}$$

where Y_A^S is the sputtering yield of the A atoms from the altered layer [23,24]. This simply derives from the constraint to sputter the material in the correct stoichiometry at equilibrium.

The second relation, derived by Sigmund, is [19,23,24]

$$\frac{Y_A^S}{Y_B^S} = \left(\frac{M_{2B}}{M_{2A}}\right)^{2m} \left(\frac{U_B^S}{U_A^S}\right)^{1-2m} \tag{15}$$

where $0 \le m \le 0.2$ and where U_A^S and U_B^S are the energies to remove A and B atoms from the compound surface. There are many other models, however Malherbe and Odendaal [25] find that Sigmund's model of equation (15) is the best description for the 13 compound semiconductors that they analysed with m optimised at 0.145. For GaAs, the ratio $K = \left(X_B^S / X_A^S\right) / \left(X_B / X_A\right)$ was found, at 0.82, to be close to the predicted value of 0.725 [25]. This prediction used Kelly's [22] expressions

for U_A^S and U_B^S, derived from pair bond theory with the assumptions of zero heat of mixing in the compound and that the system is random:

$$U_A^S = X_A^S U_A + 0.5 X_B^S (U_A + U_B) \tag{16}$$

$$U_B^S = X_B^S U_B + 0.5 X_A^S (U_A + U_B) \tag{17}$$

Here, U_A and U_B are the energies to remove A and B atoms from pure A and B. These equations are for a surface altered layer that may be more than a monolayer thick. If only Gibbsian segregation is important, then events occur in the outermost layer and, in the pair bonding approximation, U_A^S and U_B^S are closer to U_A and U_B, respectively, than shown in equations (16) and (17). The sputtering process will make the randomness assumption more valid.

If, in equation (15), m is set to zero, then from equations (14) and (15) we get Anders and Urbassek's [26] result

$$\frac{X_A^S}{X_B^S} = \frac{X_A}{X_B} \frac{U_A^S}{U_B^S} \tag{18}$$

Combining equations (16), (17) and (18), together with $X_A^S + X_B^S = 1$ and $X_A + X_B = 1$, leads to an expression for X_A^S:

$$X_A^S = \frac{\left[p^2 + \left(1 - p^2\right) X_A\right]^{0.5} - p}{1 - p} \tag{19}$$

where $p = U_B/U_A$. From equations (16) and (17), U_A^S and U_B^S may then be obtained.

Figure 1 shows how X_A^S varies with the ratio U_B/U_A (= p) for X_A = 0.2, 0.4, 0.6 and 0.8 for sputtering at equilibrium. The variation in X_A^S is significant but is not as great as one may expect since, even if U_A is very small, U_A^S only falls to $0.5U_B$. Since U_B^S then approaches U_B, X_A^S only falls to half the bulk value, X_A.

For a model of a substrate with an altered surface layer, the rate of emission of the surface atoms will largely be governed by their fraction in the surface layer and their individual binding energies. This approach may be compared with an interpolated approach as follows. In the interpolated approach, all parameters for the compound are interpolated from the values for A and B atoms as a value assigned to all sputtered atoms equally. This avoids the details of any model and the need to calculate X_A^S, X_B^S, U_A^S and U_B^S. The ratio of the yield including a simple preferential sputtering (Y_{PS}) to that from interpolation (Y_{int}) without considering preferential sputtering is now calculated. This ratio is given by:

$$\frac{Y_{PS}}{Y_{int}} = \frac{X_A^S / U_A^S + X_B^S / U_B^S}{1 / U_{int}} \tag{20}$$

where

$$U_{int} = X_A U_A + X_B U_B \tag{21}$$

Equation (20) is derived from equation (1) using the fact that the energy deposition rate is unaffected by the changes in the outermost layer and the sputtering yields in the two cases are dependent on the coverage and bonding of the atoms being sputtered.

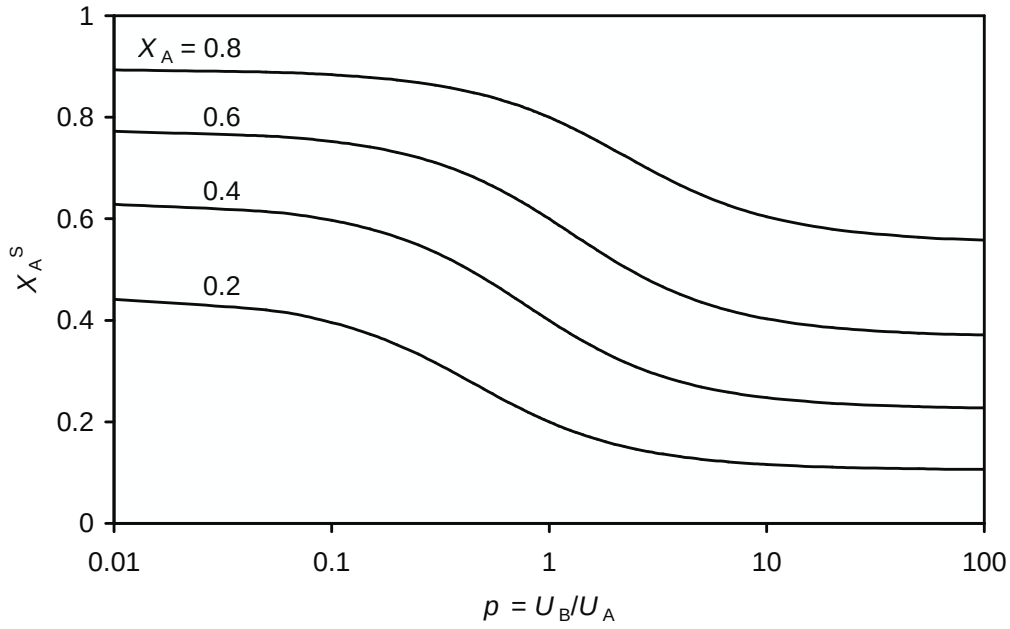

Figure 1. Variation in X_A^S as a function of U_B/U_A for X_A = 0.2, 0.4, 0.6 and 0.8.

Figure 2 shows a map for Y_{PS}/Y_{int} for changes in U_B/U_A and X_A. The sputtering yield ratio is between 0.95 and 1.0 for the central white region in which $0.4U_A < U_B < 2.5U_A$ for all X_A. Thus, for most systems, the very simple interpolated approach giving Y_{int} is within 5% of the more correct calculation with preferential sputtering at equilibrium given by Y_{PS}. Of course, the relative amounts of the constituents sputtered will be incorrect at the start of sputtering but will be correct at the equilibrium state since, at equilibrium, the whole material is sputtered in relative quantities defined by the stoichiometry. An error of 5% is generally well within experimental uncertainty of sputtering yields. It appears that the different bonding for the A and B atoms leads to a high emission of the weaker species at the start of sputtering but that the result of the preferential sputtering is that the surface composition changes to reduce the sputtering yield to close to the value for the interpolated compound. This is shown in figure 3 which plots the ratio of the sputtering yield in atoms at the start of sputtering, $Y_{PS}(0)$, to that at equilibrium, Y_{PS}, and the ratio Y_{int}/Y_{PS}, both as a function of U_B/U_A for the case of X_A = 0.5. Preferential sputtering can cause a significant change in yield between the initial and final rates even though Y_{int} is still a good approximation for the equilibrium value, Y_{PS}.

In order to understand the extent of the compositional changes, the effects of the different recoils of the constituent atoms, the radiation-enhanced diffusion, segregation and preferential sputtering need analysis [22,24,27-29]. Whilst experimental data may be fitted, the final predictive description of the preferential sputtering incorporating these effects is not yet accurate. The result implicit in figure 2 is therefore an essential aid if compound sputtering yields are to be predicted.

In all of the present work, the sputtering yields are below 10 atoms/ion. This is the yield range for the linear cascade presented here in the semiempirical approach. At higher yields, spikes occur and the yield is progressively enhanced. In sputtering with cluster primary ions, the effects of the spike need inclusion. In Seah's study [11] mentioned earlier, the spike enhancement can reach a factor of 100 when using 10 MeV Au_{13}^+, i.e. the spike then dominates the process. At these higher yields, the population of the larger sputtered fragments grows at the expense of the monatomic particles [30].

In the next section, the experimental data for GaAs and Ta_2O_5 are considered. The curves for Y_{PS}/Y_{int} for these two compounds are shown in figure 4 where for $0.4U_A < U_B < 2.5U_A$, Y_{PS}/Y_{int} is between 0.97 and 1.0. For GaAs, U_B/U_A = 1.05 and for Ta_2O_5 U_B/U_A = 0.3. Thus, Y_{int} may be taken to

be equal to the more formally correct Y_{PS} but does not require the detailed evaluations of X_A^S, X_B^S, U_A^S and U_B^S.

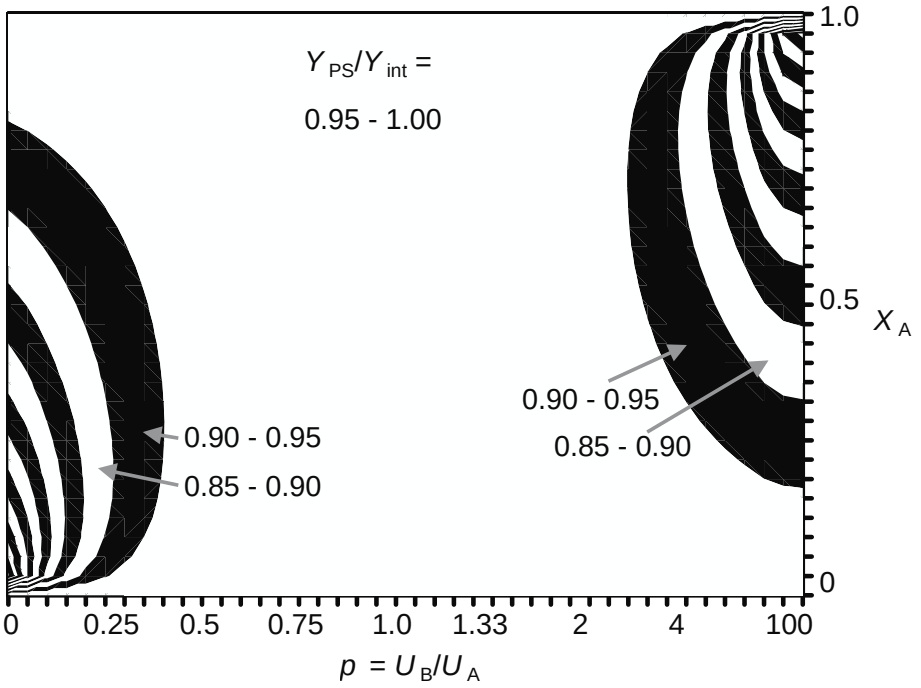

Figure 2. Contour map for the ratio of Y_{PS}/Y_{int} as a function of X_A and U_B/U_A. The bands represent successive zones of changes in the ratio Y_{PS}/Y_{int} by 0.05. Thus, the centre white zone is for Y_{PS}/Y_{int} = 0.95 to 1.00, the next black zone is for 0.9 to 0.95 and so on. The abscissa increases in U_B/U_A from 0 to 1 in increments of 0.05 for the left hand half of the diagram. The right hand reflects this symmetrically by using an equivalent scale in $1/p$ with $U_A/U_B = 0$ at the extreme right (i.e. $1/p$ increases in 0.05 increments moving leftwards).

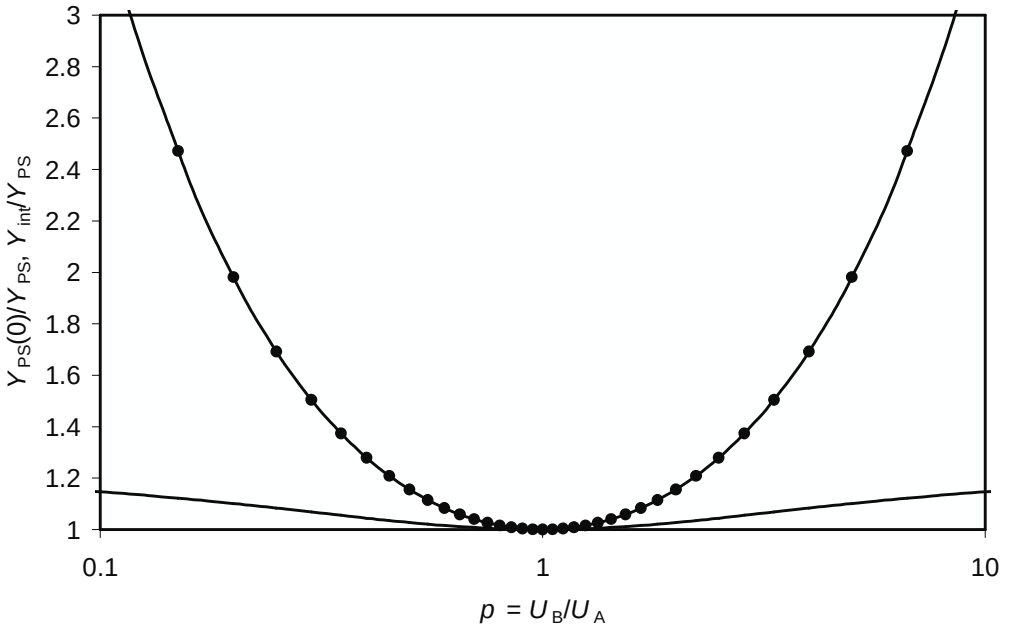

Figure 3. Ratio of $Y_{PS}(0)/Y_{PS}$ (—●—) and Y_{int}/Y_{PS} (——) as a function of U_B/U_A.

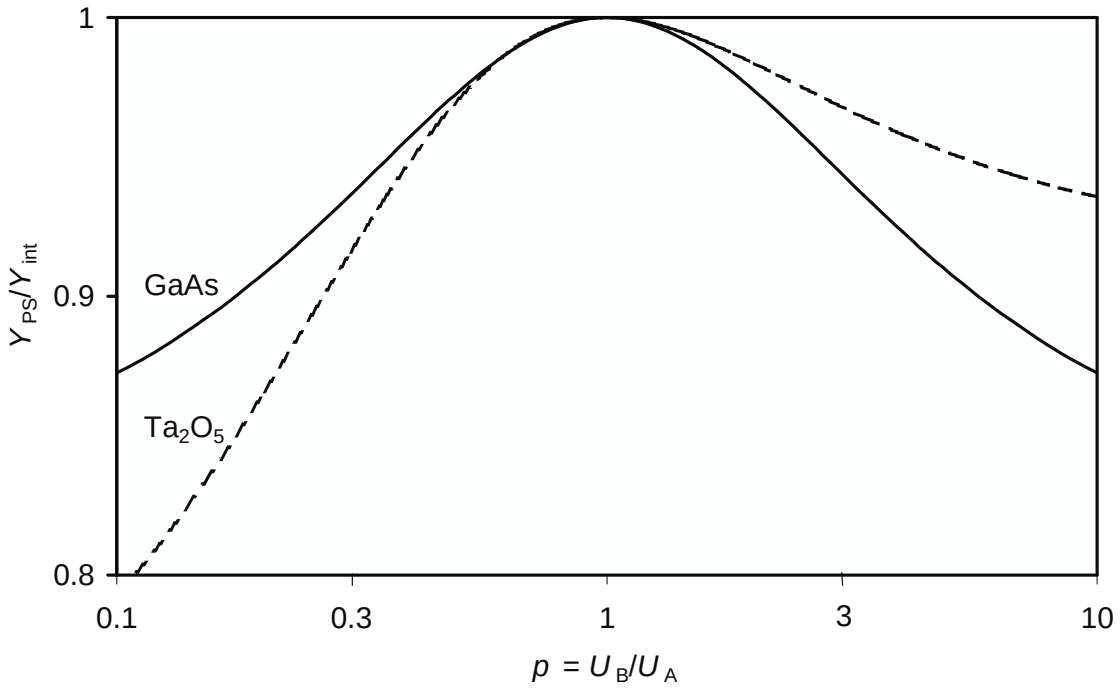

Figure 4. Ratio of Y_{PS}/Y_{int} as a function of U_B/U_A for GaAs (——) and Ta_2O_5 (------). Note the expanded ordinate scale.

3. Sputtering yields of GaAs for normally incident argon ions

3.1. The GaAs sputtering yield data

Malherbe [20] has reviewed the sputtering data for GaAs and provides a table (Malherbe's Table 5) of 60 yield values for argon ion energies between 40 eV and 35 keV. Those data are for (100), (110), (111) surfaces and polycrystalline or unstated surfaces. However, inspection shows that no significant differences are visible between these groups and so they are treated here as one group. The data, as with most sputtering yield data, show significant scatter and on a log plot show a scatter standard deviation equivalent to a factor around 1.6. The scatter is likely to be experimental scatter since the works of some 27 references are listed. To reduce the scatter, values at a similar energy may be averaged. Here, the averaging is over 5 neighbour points for the energy and the yield, except at the ends of the range where 3 points are used and the final result, unaveraged, is discarded. The points are sufficiently close that arithmetical and geometrical averages are very close. Here, a geometric average is used since the scatter appears to be symmetrical in log space. These averaged sputtering yield data are shown in figure 5. The data give a significantly more sensitive test for a prediction of the yield than the original, unaveraged data shown in the plots presented by Malherbe [20].

A predictive yield may be calculated from equations (1) to (13) directly using values interpolated mid-way between the values for Ga and As for each of the parameters to use in equation (1) rather than calculating them from the average atomic numbers and average masses. Here, U_o(Ga) = 2.819 eV/atom and U_o(As) = 2.970 eV/atom [31] (Note: for those without access to reference [31], many of the values are very close to those of reference [32]). The curve for this result is shown in figure 5(a). This shows both the correct shape and an average ratio for the data to the prediction of 1.01 with a standard deviation of 0.11 and a standard deviation of the mean of 0.01. The rapid fall in yield at low energies confirms that equation (11) correctly estimates E_{th}. The whole curve shows remarkably good fit with theory over almost 2 decades of yield with only 11% standard deviation. It should be noted that, in calculating the sputtering yield in this way, the following have been ignored; any change in lattice size as a result of forming the compound GaAs, the effect of the reaction with its associated heat of mixing and finally, through figure 2, any effect of preferential sputtering.

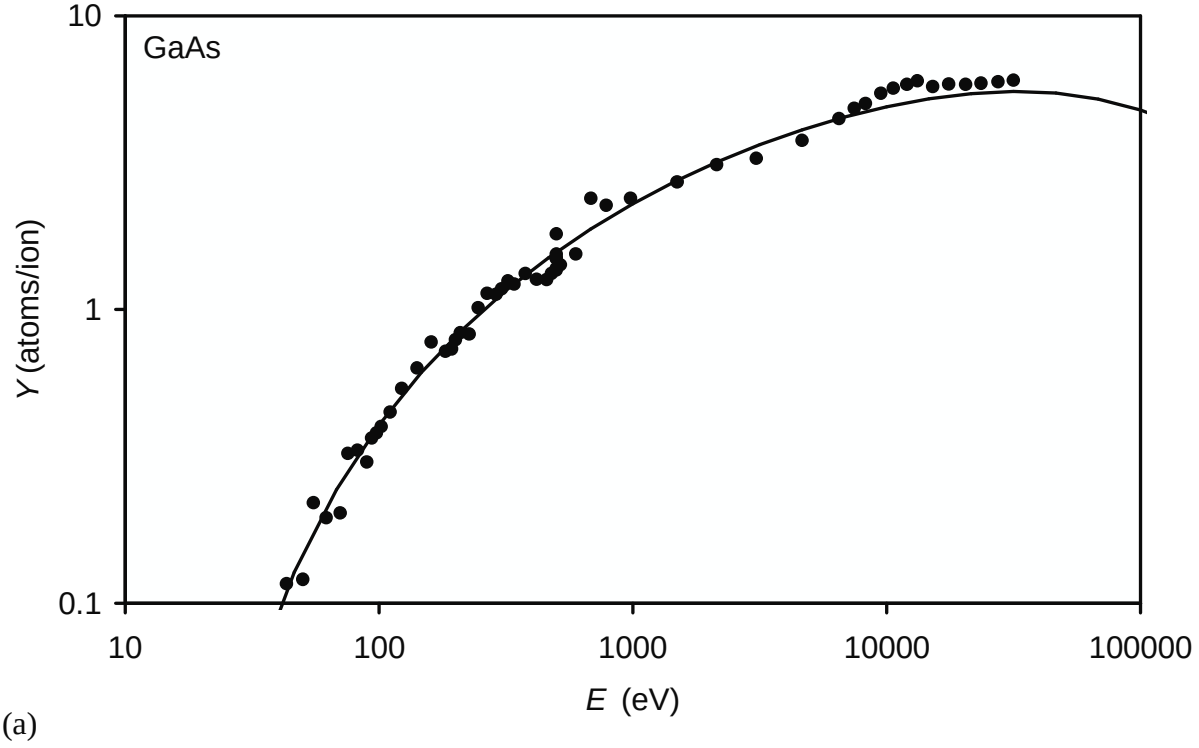

(a)

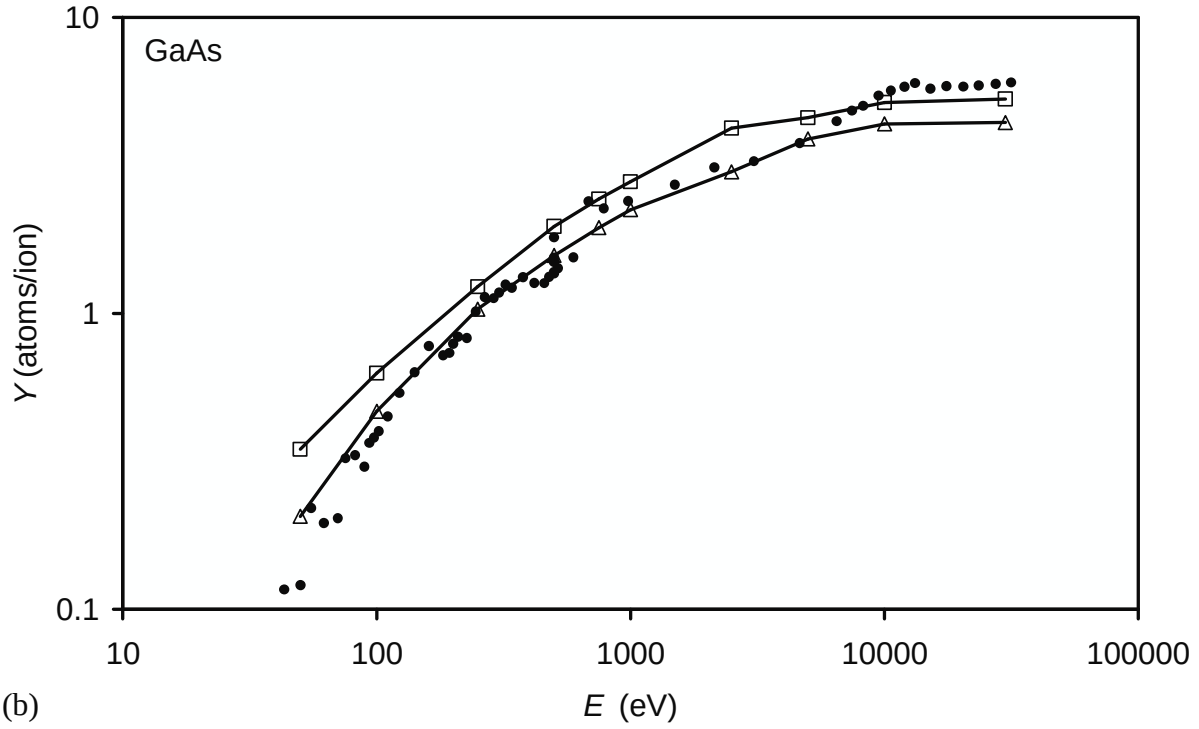

(b)

Figure 5. Sputtering yield data for GaAs using argon at normal incidence. The data (•) are from Malherbe's [20] Table 5, averaged over 5 neighbouring points except for the end points. Note that the ordinate is in atoms/ion whereas Malherbe [20] uses molecules/ion. (a) the curve shows the result of the semi-empirical theory with interpolated parameters and ignoring the effect of H_{AB}, (b) the upper line (□) is for SRIM 2006 for the total number of atoms sputtered per argon ion using the mean atomic number $Z = 32$ with density 5.31 g/cc and $U_o = 2.895$ and the lower line (Δ) for SRIM 2006 for material of 50% Ga and 50% As with density 5.31 g/cc and U_o (Ga) = 2.819 eV, U_o (As) = 2.970 eV.

3.2. Analysis of the effects of compound bonding

From the above U_o values, one would expect the Ga to be depleted slightly at the surface but observation indicates that the reverse is the case [25] with a small enhancement averaged over the AES or XPS sampling depths. The Ga enrichment appears to arise from depletion relative to an underlayer that is Ga rich. These effects do not change the energy deposition rate that controls the sputtering. Intuitively, one may expect As to be depleted since it easily evaporates but that is an erroneous view. From solid As it is As_4 that evaporates and not the monatomic As emitted from GaAs. As_4 requires only 0.398 eV/atom, whereas As_2 requires 0.988 eV/atom and As requires 2.970 eV/atom [31]. Thus, whilst the evaporation of arsenic is relatively easy, the evaporation of monatomic As is much harder with U_o(As) = 2.970 eV/atom, a value similar to U_o(Ga).

So, in a practical sense, details of the model may be incorrect but the robustness of the Y_{int} result from figures 2 and 4 shows these details to be relatively unimportant for the equilibrium sputtering yield. From equations (18) to (21) for GaAs where $X_A = 0.5$:

$$\frac{Y_{PS}}{Y_{int}} = \frac{U_A + U_B}{U_A^S + U_B^S} \tag{22}$$

hence

$$\frac{Y_{PS}}{Y_{int}} = \frac{U_A + U_B}{0.5U_A + 1.5U_B + (U_A - U_B)\, X_A^S} \tag{23}$$

This ratio remains very close to unity, even for large changes in the surface composition X_A^S arising from preferential sputtering. This may be seen using the approximation that $U_B = U_A(1 + \delta)$, when

$$\frac{Y_{PS}}{Y_{int}} \simeq 1 - \frac{\delta^2}{16} \tag{24}$$

irrespective of the value of X_A^S.

We should now consider the difference in density from that used in the interpolation between both Ga and As (5.816 g/cc) and that of GaAs with density 5.315 g/cc. These methods give r as 0.274 and 0.283 nm, respectively. Although this change is small, the effect, through equation (12) would be to scale the predicted sputtering yield by a factor of 0.92.

A second term ignored above is the heat of mixing, H_{AB}, per atom. From calculations from the MTDATA software [31] for the reaction

$$GaAs \leftrightarrows Ga(g) + As(g) \tag{25}$$

an average value of U_o per atom of 3.355 eV is obtained. This is slightly higher than the 2.895 value obtained by interpolation from equation (21) and is very close to the value used by Malherbe [20]. Equation (21) is now replaced by

$$U_{int} = X_A U_A + X_B U_B + H_{AB} \tag{26}$$

This increase in U_o through an H_{AB} value of 0.46 eV per atom affects the yield directly through equation (1) and less directly through equation (11). The calculated shift in E_{th} from 12.4 eV to 14.4 eV is, unfortunately, not enough to prove that either one is incorrect from the data of figure 5(a). The effect of the increase in U_o is to scale the yield through equations (1) and (11) by a further factor of ~ 0.85. Damage from the argon and the preferential sputtering both serve to move the material away from the energy minimum and crystal structure associated with stoichiometric GaAs and more towards an amorphous structure with a random array and a lower heat of mixing. The contribution of the heat of mixing thus scales the sputtering yield by a factor between 1.00 and a lower limit of 0.85,

associated with the incorporation of the thermodynamic value of H_{AB} into the calculation. For a reacting system, one could write, in analogy with equations (16) and (17):

$$U_A^S = X_A^S U_A + 0.5 X_B^S (U_A + U_B) + X_B^S H_{AB} \quad (27)$$

and

$$U_B^S = X_B^S U_B + 0.5 X_A^S (U_A + U_B) + X_A^S H_{AB} \quad (28)$$

However, such equations do not fully describe the observed phase diagram [33,34]. The value of H_{AB} of 0.46 eV/atom is valid at the very sharp minimum at GaAs but is significantly smaller than this away from stoichiometry. Thus, the effective value of U_{int} is better given by

$$U_{int} = X_A U_A + X_B U_B + x H_{AB} \quad (29)$$

where $0 \leq x \leq 1$. The sputtering yield is now much closer to the upper limit with $H_{AB} = 0$ than that using the equilibrium thermodynamic value of H_{AB}.

In a similar way, the SRIM code [35] may be used to calculate the sputtering yield either using the suggested average value, $Z = 32$ [20] with the bulk density of 5.315 g/cc or, better, for the compound GaAs with the same density but with U_o(Ga) = 2.819 eV/atom and U_o(As) = 2.970 eV/atom. SRIM is used here as it is widely available, clearly documented and is popularly used. It is therefore helpful to relate the present calculations to that system. Note that the default SRIM values [35] are 2.82 eV/atom and 1.26 eV/atom, respectively; Malherbe [20] uses U_o(As) = 1.24 eV/atom and low values may be found on the web. MTDATA [31] gives the data cited earlier and it is a is mixture of these that gives the readily observed sublimation and the low U values sometimes cited. The SRIM sputtering yields for the compound GaAs, shown in figure 5(b) are, as expected, better than the SRIM sputtering yields for the average atomic number $Z = 32$ but are still not as good the semi-empirical equation. The prediction using SRIM shows a slightly weaker energy dependence and a different low energy behaviour. The ratio of the data to the prediction here is 1.01 ± 0.28 (lower curve in figure 5(b)), a scatter rather worse than for the semi-empirical equation and arising from the different energy dependence. Note that SRIM provides the number of each species removed from the stoichiometric surface but not that at dynamic equilibrium. It gives slightly more Ga atoms sputtered than As. SRIM provides calculations for the trajectories of ions with some sophisticated detail in the physics of transport and so provides accurate details of ranges, recoil mixing, transport parameters and so on but sputtering yields are less accurate.

Next, the very different system of tantalum pentoxide is considered.

4. Sputtering yields of Ta_2O_5 for normally incident argon ions

4.1. The Ta_2O_5 sputtering yield data

A consistent set of argon ion sputtering yield data for Ta_2O_5 has been published by Hunt and Seah [36] in the development of the reference material BCR 261 [37]. The sputtering yield at normal incidence in atoms/ion is given in figure 6(a). The energy range of the data is somewhat smaller than in figure 5 and so the data are shown on linear axes in figure 6. As for GaAs, the sputtering yield for Ta_2O_5 is first calculated from the semi-empirical theory by interpolating between the sputtering for O and Ta but using the bulk density of 8.2 g/cc since the density of O_2 is significantly different from that of oxygen in compounds. Note that E_{th} for oxygen and for tantalum are 29.9 and 29.3 eV and, as described above, the interpolation is made between these values and not between the E_{th}/U_o values in order to deduce a value for E_{th}.

Allowance for the change in composition of the surface layers may be made. Of course, Ar is implanted in the surface layer as it is in all equilibrium sputtering measurements [4]. This implantation will both reduce the effective U_o and change the density. However, these effects are thought to be incorporated in the semi-empirical Q values determined earlier [4]. Note also that here

the preferential sputtering is sufficient to reduce the average composition seen by AES [36,38-40] to Ta_2O_4 at the higher ion energies and Ta_2O_3 at the lower energies, and similarly by XPS [41]. Incidentally, the calculation leading to figure 1 also predicts a composition of Ta_2O_3 for the altered layer. For bulk solids of Ta_2O_4 and Ta_2O_3 composition, the interpolated value of U_o increases by 6% and 15%, respectively, from the value for Ta_2O_5. Hence the sputtering yields fall similarly, as shown by the dashed and dotted lines in figure 6(a). These are not as close to the data as the interpolated calculation based on the bulk composition. From figure 6(a), it seems that a direct calculation, ignoring the preferential sputtering, achieves the best result. The ratio of the measurements to the semi-empirical theory is then 1.00 ± 0.07.

4.2. Analysis of the effects of compound bonding

Again, the heat of reaction, H_{AB}, may be considered. H_{AB} has a value of 3.008 eV/atom which, ratioed to the binding energy for Ta_2O_5, U_{Ta2O5}, is 0.718. Applied directly, this would reduce the sputtering yield by a factor of 1.718 but it is clear that this reduction is much weaker in practice since, as for GaAs, the sputtering and disorder moves the binding energy away from the sharp minimum of the stoichiometric compound. The semi-empirical theory with interpolated parameters, $H_{AB} = 0$, and the bulk density gives the best fit with the experimental data as it did for GaAs.

For comparison, in figure 6(b), the SRIM results are plotted as in figure 5(b) for an average atomic number for Ta_2O_5 close to that of cobalt with density 8.2 g/cc and the interpolated $U_o = 4.187$ and also for Ta_2O_5 with the separate elements Ta and O with the above values of density and U_o. As before, using an average matrix leads to a significantly raised sputtering yield but the SRIM predictions for the correct matrix are better, being only 23% too high. Using equations (16) and (17) for separate U_{Ta}^{S} and U_{O}^{S} values gives a result within 1% of that for the average matrix, as expected from figure 2. The ratio of the SRIM 2006 calculation to the experimental data is 1.23 ± 0.06. Again, the SRIM analysis is not at equilibrium but for the interpolated binding energy and for the separate binding energies, respectively, the oxygen atoms are being sputtered at 0.6 and 1.2 times as fast, per atom, as the Ta atoms.

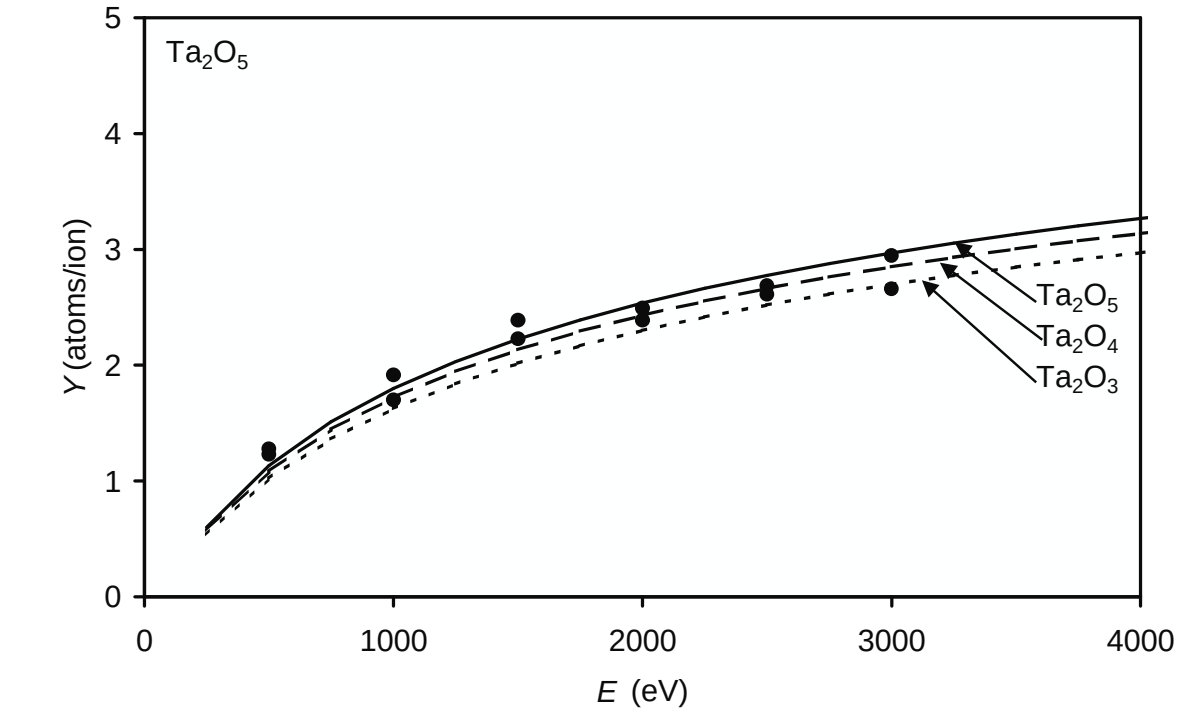

(a)

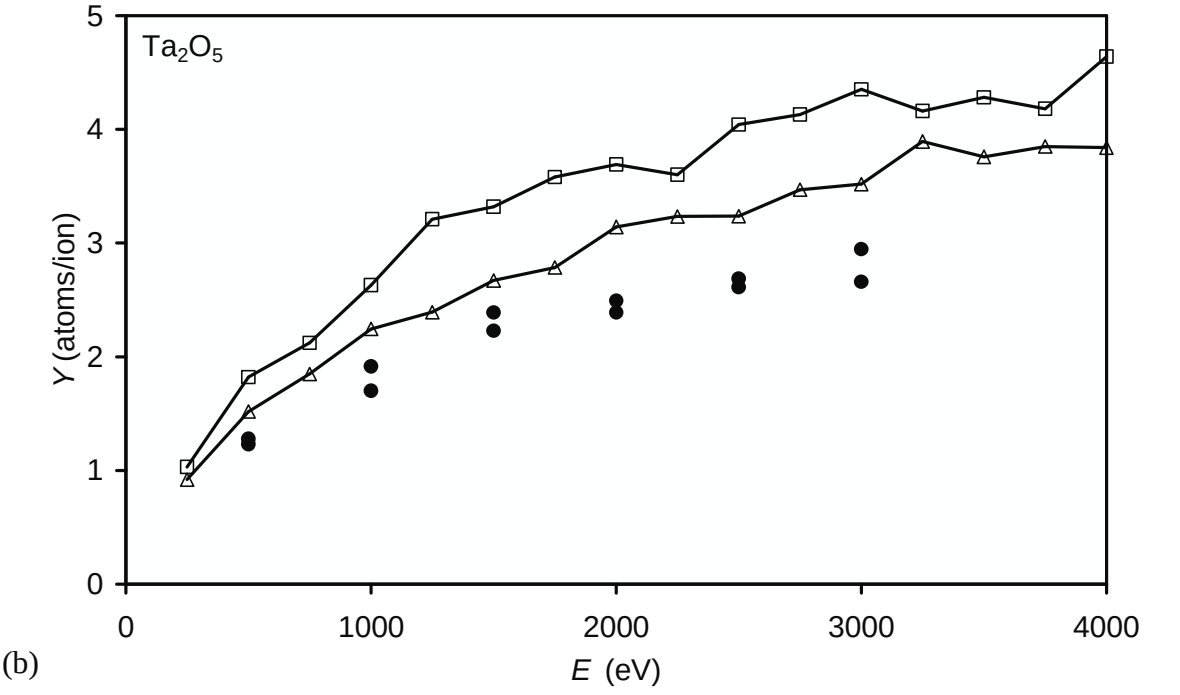

(b)

Figure 6. Sputtering yield data (●) for Ta_2O_5 using argon at normal incidence from Hunt and Seah [36]. The ordinate is again in atoms/ion. In (a), the continuous curve (——) shows the result of the semi-empirical theory with interpolation and a bulk density of 8.2 g/cc, the dashed (------) and dotted (·····) curves are for Ta_2O_4 and Ta_2O_3 with interpolations from the Ta_2O_5 bulk density, respectively. In (b), the upper line (□) is for SRIM 2006 for the average atomic number $Z = 27$ with density 8.2 g/cc and $U_o = 4.187$ eV and the lower line (Δ) for SRIM 2006 for Ta and O atoms in Ta_2O_5 with density 8.2 g/cc and U_o (Ta) = U_o (O) = 4.187 eV.

5. Sputtering yields of other oxides for normally incident argon ions

There are many other measurements for sputtering yields but it is not productive to analyse all since, for instance, the individual data generating figure 5(a), which are typical of sputtering yield data, scatter by a factor of 1.6 with the outliers reaching a factor of 5. Absolute sputtering yield experimental data are not generally of good quality. Of particular interest are thin layers of oxides grown on substrates by thermal oxidation or by anodic oxidation in laboratories dealing extensively with those systems. Often such data are measured as a sputtering rate referenced to Ta_2O_5 or SiO_2 reference standards to avoid the need to measure the ion beam current density. There are few data to test the Ta_2O_5 model described earlier to significantly higher or lower energies but references [42] to [45] contain significant sets of sputtering yield data for Al_2O_3, Cr_2O_3, FeO, Fe_3O_4, Fe_2O_3, Nb_2O_5, NiO, SiO_2, Ta_2O_5, and ZrO_2. Recent measurements provide data also for CeO_2, TiO_2 and ZnO sputtering rates relative to SiO_2 [46]. SiO_2, as the only other reference material, will be considered at greater length in the next section.

For each of the above oxides, the sputtering yields for the compound may be calculated ignoring preferential sputtering and using the interpolated U_{int} as an upper limit for the sputtering yield and then, also, by reducing that yield by $[1+(H_{AB}/U_{int})]$ to give a lower limit that fully includes the heat of reaction. The values for these parameters are given in table 1 for convenience. The energy dependence of the sputtering yield will be correct unless there is a significant energy dependence of the preferential sputtering and H_{AB}/U_{int} is large. Thus, the ratios of the experimental data to the calculated yields may be evaluated for any energy and be compiled onto one plot for the ratios of measurement to calculation.

Figure 7(a) shows the compilation of data for the average ratio of the measurement to the calculations for each compound, ignoring the heat of mixing, H_{AB}. The horizontal line at unity would represent a good correlation. If H_{AB} is fully included, the calculated values progressively diminish and the ratio would rise. The position of the correlation line amongst the data then follows the dashed line. This clearly fits some of the data better than the horizontal line. As noted above, the real situation will be somewhere between these extremes and so between the dashed and solid lines which may be treated as upper and lower bounds. The error bars are for one standard deviation of the means rather than the larger standard deviations of the individual measurements since we wish to have a measure of the meaningfulness of the means. Figure 7(a) shows that the oxide data do fit between the two extremes noted above with Nb_2O_5 and Ta_2O_5 showing correlation with $H_{AB} = 0$ and the others requiring a significant part of H_{AB}. From the above simple theory, if the preferential sputtering reduced the compound AB to be A_3B in the altered layer, the effect of H_{AB} would be, at least, halved (i.e. $x < 0.5$ in equation (29)). Thus, the position of compounds between the two extremes depends on the extent of the preferential sputtering in the altered layer. Those showing little preferential sputtering fall towards the dashed curve and those showing extensive preferential sputtering rise towards the horizontal line. Data on the preferential sputtering are given by Malherbe *et al.* [47] for all of these compounds except NiO and CeO_2, as shown in the bottom row of table 1 by the ratio of ratios $(X_M/X_O)_s/(X_M/X_O)_b$. From these data, the fraction x of the relevant compound, say A_aB_b, to be mixed with either A or B, to obtain the measured composition after sputtering, may be calculated. This modifies the effect of H_{AB} by the factor x. Malherbe *et al.*'s data are mainly for AES where the electron energy is such as to sample about 4 monolayers. If the preferential sputtering is mainly in the outermost layer, this sampling effect would enhance the shift from AB towards A by a factor of 4 compared with the spectroscopic ratios given by Malherbe. In this way, figure 7(b) shows the ratio of the experimental sputtering yield to the calculated value where U_{int} has been replaced by $(1 + xH_{AB}/U_{int})U_{int}$ where x is $(1 - 4\{1 - [(X_O)_s/(X_O)_b]\})$ or 0 if $(X_O)_s/(X_O)_b \leq 0.75$. For NiO and CeO_2, in the absence of experimental data, the values of $(X_O)_s/(X_O)_b$ are taken as unity. Figure 7(b) is a significant improvement on figure 7(a) and removes the major dependence seen there. The standard deviation of the data in figure 7(b) is 16%. This is, for absolute sputtering yield data, an excellent result. The SiO_2 data are now analysed more closely since SiO_2 is often used as a reference material.

Table 1. Values of parameters for the oxides.

	Al_2O_3	CeO_2	Cr_2O_3	FeO	Fe_3O_4	Fe_2O_3	Nb_2O_5	NiO	SiO_2	Ta_2O_5	TiO_2	ZnO	ZrO_2
H_{AB} (eV/atom)	3.45	3.74	2.34	1.40	1.64	1.65	2.79	1.22	3.12	3.01	3.20	1.80	3.78
U_{int} (eV/atom)	2.94	3.19	3.22	3.45	3.34	3.29	4.01	3.51	3.30	4.19	3.38	1.98	3.82
H_{AB}/U_{int}	1.17	1.17	0.73	0.40	0.49	0.50	0.69	0.35	0.94	0.72	0.95	0.91	0.99
$(X_M/X_O)_s/(X_M/X_O)_b$	1.00		1.00	1.05	1.05	1.05	2.22		1.00	2.5	1.50	1.00	2.26

6. Sputtering yields of SiO_2 for normally incident argon ions

6.1. The SiO_2 sputtering yield data

Data for SiO_2 are more extensive than for the other oxides and values from references [48] to [61] are shown in figure 8. The results from Mogi *et al.* [61] are for a study between 7 laboratories for measuring the relative sputtering rates of Si and SiO_2. This is converted to the SiO_2 sputtering yield using the Si sputtering yield calculated according to reference [3] and the bulk densities. The smooth solid curve is for the calculated semi-empirical sputtering yield using the result formulated above and the data for SiO_2 in table 1. This is the same as a full correction for H_{AB} since $x = 1$ for SiO_2. The smoothed dashed line is for the semi-empirical sputtering yield with $H_{AB} = 0$.

The experimental data are somewhat scattered and form a lower band containing much of the individual data, a middle band for the data of Tu *et al.* [58] and an upper band for the low energy data of Jorgenson and Wehner [49]. The data from Viefhaus *et al*. [45] cover the two lower bands. In the analysis for figure 7, the average used does not include the data of Jorgenson and Wehner that are at very low energy. Most of the data in figure 8 are for bulk SiO_2, probably with density 2.32 g/cm^3, rather than the thin thermal oxides on wafers studied today with density 2.196 g/cm^3. The present calculations are all for a consistent density of 2.196 g/cm^3 and will therefore be some 6% lower than calculations for the higher density. This difference is less than the size of the plotted points. The asterisk points joined by straight lines are the calculations from SRIM 2006 [35] for a density of 2.196 g/cm^3 using the default binding energies for Si and O of 4.7 eV and 2 eV, respectively. These lead to different yields for the Si and O atoms so that non-stoichiometric sputtering occurs (as in $Y_{PS}(0)$) with a high rate for the oxygen. The plotted points are for the sum of these individual atomic yields. This initial rate, as noted earlier, will decrease with time as the preferential sputtering, damage layer and argon incorporation become established so this could be taken as an upper limit. That there is preferential sputtering of oxygen is discussed by Smentkowski [62] in relation to experiments in which oxygen is added to the argon, causing the sputtering rate to fall significantly. However, this does not agree at all with surface analysis data as summarised by Malherbe *et al*. [47] and shown in table 1. If the default binding energy values are replaced by the U_{int} value shown in table 1, the results joined by the thin black line, close to the semiempirical model including H_{AB}, are obtained using SRIM 2006. Relative to the semiempirical model, the SRIM energy dependence gives slightly higher data at very low and at very high energies. The SRIM results for U_{int} are very close to the semiempirical results including H_{AB}.

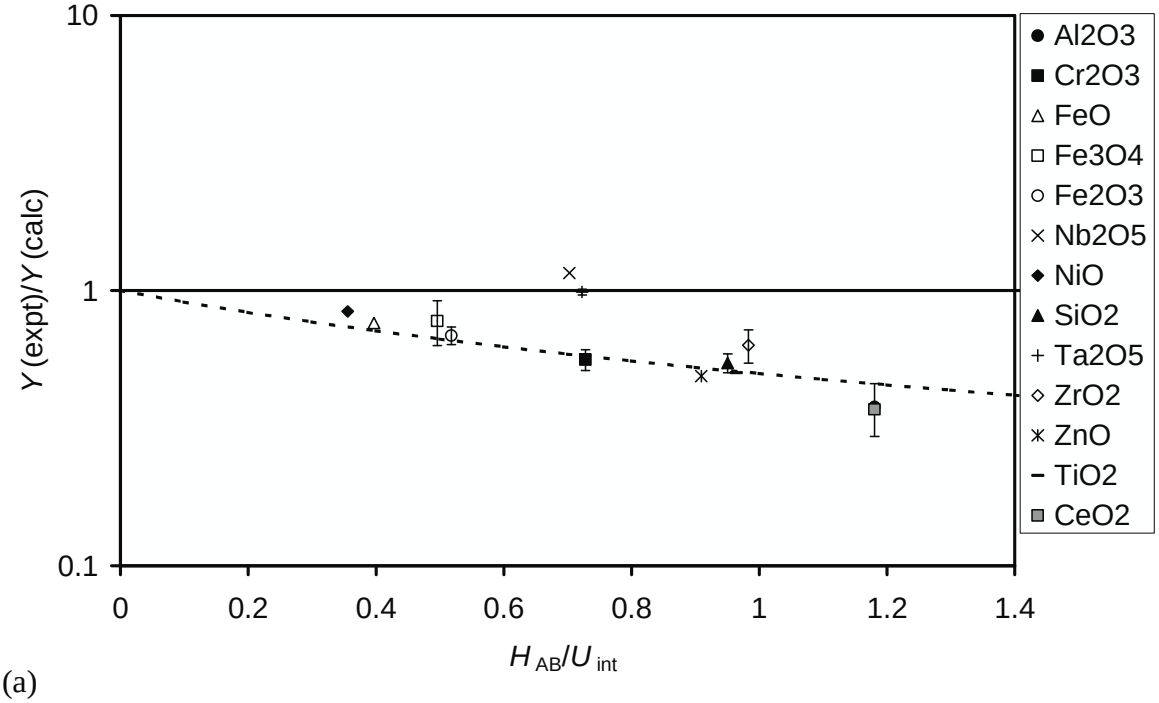

(a)

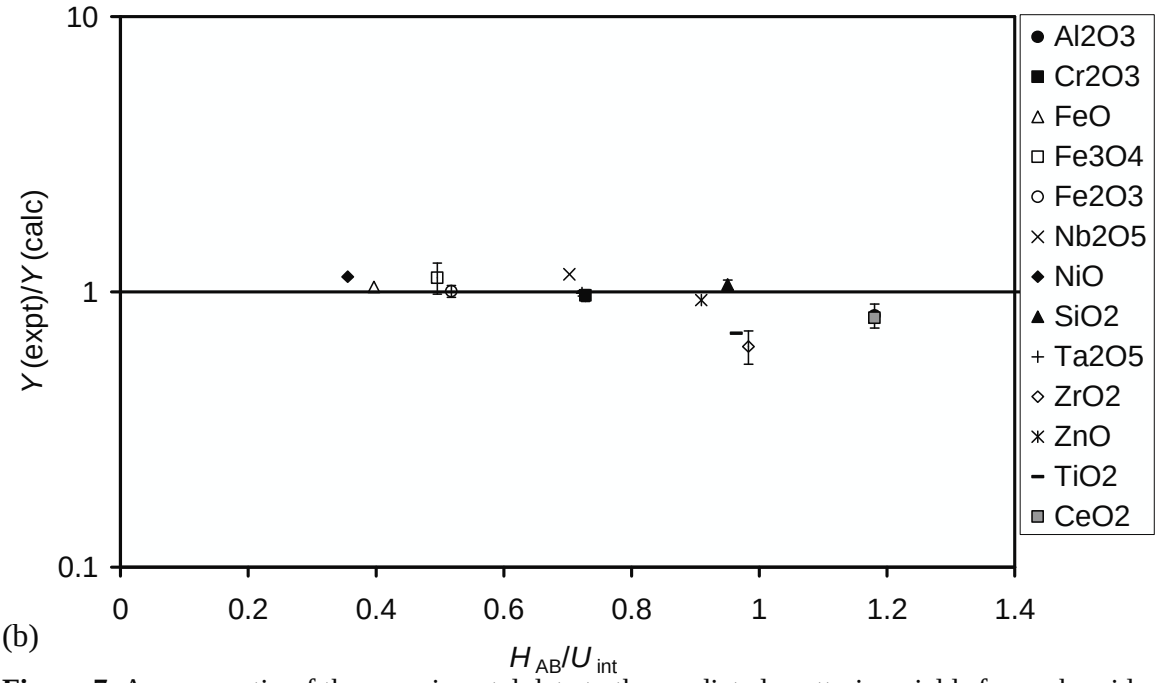

(b)

Figure 7. Average ratio of the experimental data to the predicted sputtering yields for each oxide with standard deviation of the mean error bars. In (a), the sputtering yields have been calculated with H_{AB} = 0, so the data should fall on the (——) correlation line if H_{AB} = 0 is correct, or on the (------) correlation line if H_{AB} should be fully included, In (b), the sputtering yields have been calculated with partial inclusion of H_{AB}, as discussed in the text. Viefhaus *et al*'s [45] values have not been scaled by cos(35º) to allow for their 35º incidence geometry since this effect is offset by their current density through the surface being cos(35º) times their fluence.

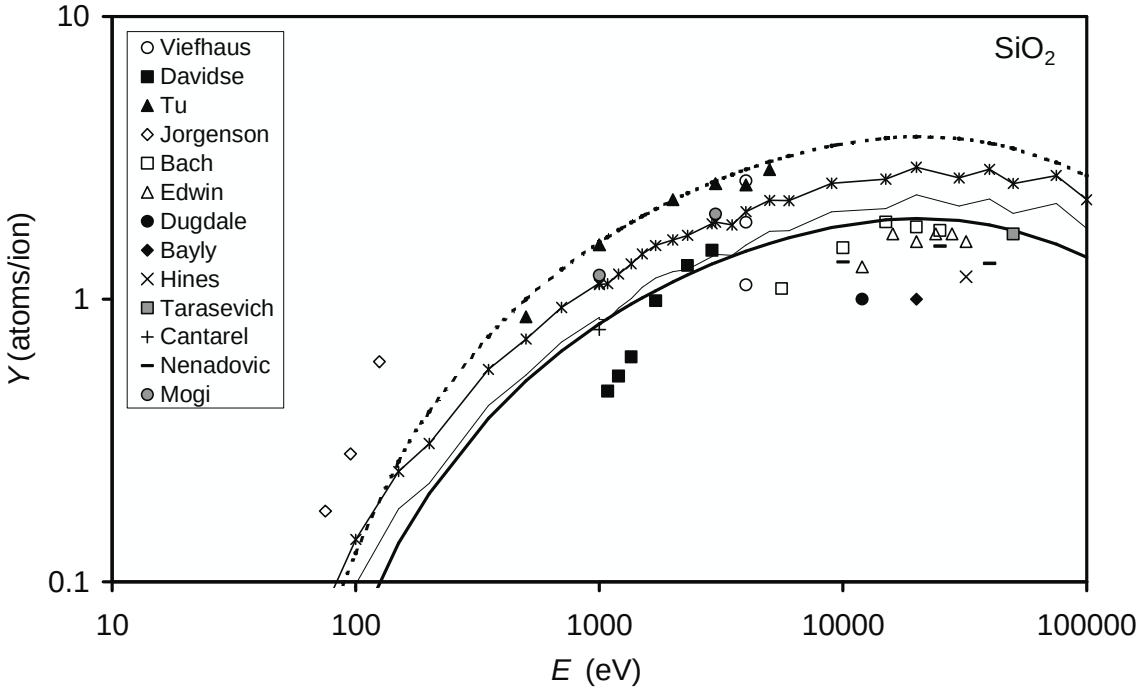

Figure 8. Compilation of published sputtering yields for SiO_2 using Ar ions from references [45-61] converted to atoms/ion. The solid line (━━━) is for the calculated yield incorporating the correction for H_{AB} (x = 1 for SiO_2) and the dashed line (------) is for H_{AB} ignored. The thin line (—✳—) is for SRIM 2006 with the SRIM default values for the binding energies and simply adds the Si and O atoms sputtered although the O atoms are preferentially sputtered by a factor of 2.1. The lower thin line (——) is for SRIM 2006 with the interpolated U_o shown in table 1 when the O atoms are preferentially sputtered by a factor of 0.9. Tu *et al*.'s [58] values have been scaled by cos(30º) to allow for their 30º incidence geometry.

The ratio of the experimental data excluding Jorgenson and Wehner's data to the semiempirical theory with H_{AB} is 1.06 with a scatter factor of 1.5 (a scatter factor is the standard deviation evaluated in log space and is useful if scatters are large and symmetric in log space) or, if the standard deviation of the mean is used, 1.06 ± 0.07. This agreement looks impressive but it is clear that, at the present time, the scatter of experimental data for SiO_2 seems very high for its use as a reference standard [63] or to be used to validate the predictions from the different methods for computing sputtering yields.

At this point there is clearly a need for improved measurements for the sputtering yield of SiO_2.

6.2. The new SiO_2 sputtering yield measurements

We therefore conducted experiments using thermal oxide grown on (100) Si wafers. Two samples were chosen, one of 30.8 nm thickness and one of 4.5 nm with the thicknesses measured by ellipsometry and XPS [64]. The sputtering yield is known to change [64] in the first layers as any preferential sputtering, damage and implantation are established and so the sputtering yield would be deduced from the time and thickness differences established with these two samples. Rate changes are well established in secondary ion mass spectrometry (SIMS) where reactive ion beams such as O_2^+ are used [65] but are still significant where unreactive ion beams are used.

Sputter-depth profiles were measured using a Thermo Scientific K-Alpha X-ray photoelectron spectrometer (XPS) that permits careful depth profiling using argon ions whilst monitoring the XPS intensities generated using monochromatic Al Kα X-rays. Considerable work has been done in the past using Auger electron spectroscopy (AES) which gives excellent profiles. However, there are indications that the sputtering is enhanced [66,67] by the presence of the electron beam of the AES and so XPS was considered more reliable. A special sample mount allowed sputtering at normal incidence for energies between 200 and 2500 eV. The time to the interface could be followed using

the O1s peak or the Si 2p oxide peak or the ratio of the Si 2p oxide intensity to the total Si 2p intensity where the total Si 2p intensity is the sum of Si 2p oxide and Si 2p elemental peak areas. These areas were determined after subtraction of a Shirley background. The three measures gave similar times to the interface and results that are closely modelled by a Gaussian depth resolution.

The use of the O 1s peak may be misleading since there may be an initial fall in intensity that is not caused by preferential sputtering but arises from the removal of surface chemisorbed water at the start of sputtering [68]. In the present work, the contamination level was very low and so there is no significant rise in intensities at the start associated with contamination removal. A small, 7%, fall in O 1s level is seen at the start whereas the ratio of the Si 2p oxide intensity to the total Si 2p intensity changes by less than 1%. This indicates, in agreement with Malherbe [47] that the preferential sputtering is negligible for SiO_2.

The time to the interface, *t*, is thus given by the time to reach 50% of the initial plateau value. This is straightforward for the 30.8 nm samples as shown in figure 9 for the data using 2500 eV argon ions, but those of 4.5 nm are too thin to show any initial plateau. For this and the above reason, the ratio of the Si 2p oxide intensity to the total Si 2p intensity is used since the plateau value for thick samples is very close to unity (0.98) whereas the absolute values for the O1s or Si 2p oxide intensities, required to evaluate the 50% position, may vary from sample to sample (the samples were analysed over 12 months). The two interface times, $t_{4.5}$ and $t_{30.8}$, were evaluated by least squares fitting to the data at the interface.

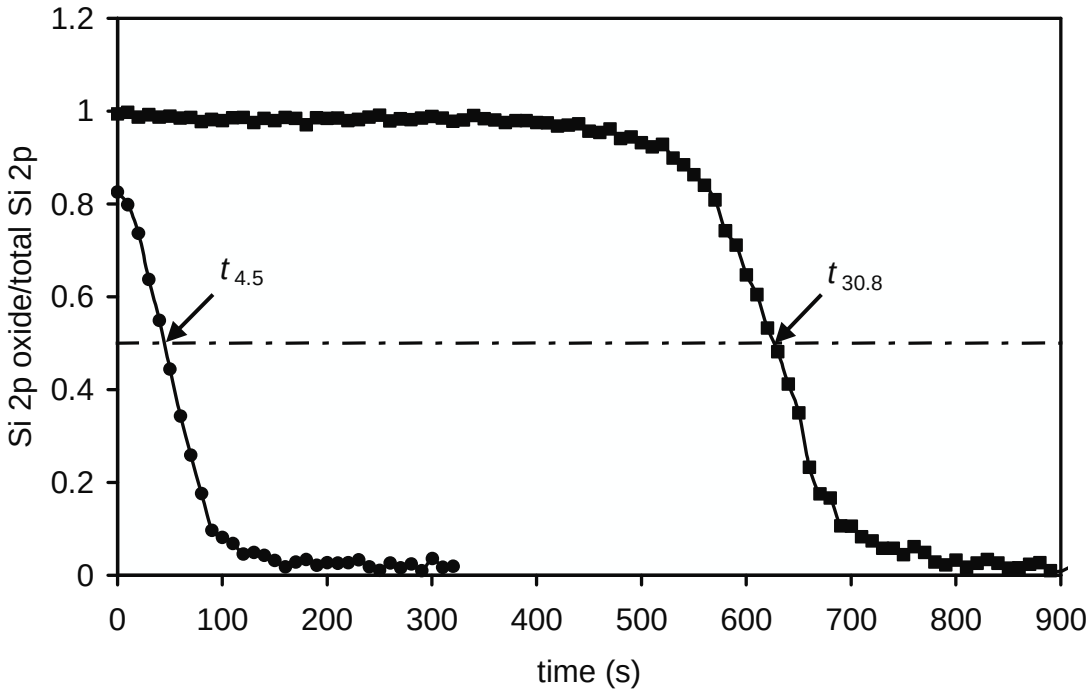

Figure 9. Depth profiles of the 30.8 nm and 4.5 nm oxides using the ratio of the Si 2p oxide intensity to the total Si 2p intensity, showing the times $t_{30.8}$ and $t_{4.5}$ determined at the 50% ordinate level.

To calculate the sputtering yields, the current density is required. Here a 3 mm by 3 mm Faraday cup, set normal to the spectrometer axis and at 58° to the ion beam axis, is used to measure the ion beam current, *I*. The raster area, *A*, is then measured by analysing the crater shape for craters where the sputtering time is approximately twice that required to reach the interface. The width is measured using optical reflectance in a calibrated optical microscope. This is faster than, but was checked to give the same result as, mapping spectroscopic ellipsometry. If the sputtering time to reach the interface is exactly 0.5 times the total sputtering time, the raster area is given accurately by the width and height of the raster area from the optical reflectance image. If the time fraction is not 0.5, a correction must be applied. If the fraction is greater than 0.5, the measured area will be too small and vice versa. The correction is easy to calculate for an assumed Gaussian beam profile but depends on the beam full width at half maximum (FWHM) intensity. This, in turn, may be determined from the

radius of the corners of the crater from the reflectance image. In this work, the corrections ranged from –0.3 to 0.1 mm for crater dimensions of typically 2.8 mm using beam FWHMs of typically 0.5 mm. This beam size is close to the maximum that can be used with the 3 mm by 3 mm Faraday cup at 58º.

The sputtering yield, Y, per atom is then calculated in the usual way using

$$Y(d) = \frac{edA}{Ita^3} \tag{30}$$

where e_o is the electronic charge and a^3 is the average atomic volume in SiO_2. This relation gives values for the sputtering yield averaged over the depth d. The values used in the work described earlier, for significant amounts of sputtering, will be close to that for equilibrium sputtering, $Y(\infty)$. To determine $Y(\infty)$, in equation (30), d is replaced by the thickness difference 30.8 - 4.5 nm and by the time difference $t_{30.8}$ - $t_{4.5}$ since the equilibrium, estimated from SIMS data for SiO_2, is reached by the 4.5 nm depth. The ratio, $Y(4.5)/Y(\infty)$, is found to be 1.83 ± 0.24 with no significant energy dependence over the energy range 200 to 2500 eV. This lack of variation with energy means that the semiempirical theory with interpolation and ignoring preferential sputtering is more likely to be valid. The change in sputter rate with depth means that the value of $Y(\infty)$ is some 7% lower than if equation (30) had been applied directly to the data for the 30.8 nm samples. The ratio $Y(4.5)/Y(\infty)$ is expected to be above unity from considerations such as figure 3. Of course, this is lower than $Y(0)/Y(\infty)$ since the yield will fall even over this thin layer.

The values of $Y(\infty)$ are shown in figure 10 together with the semi-empirical curve for $H_{AB} = 0$ and that curve scaled by 0.81. This is the same as the curve including xH_{AB} with $x = 0.25$. The data scatter about this curve with a standard deviation of 9% with, probably, equal error contributions from the measured values of A and I. These sputtering yield data are near the upper limit of the data in figure 8 being between the data of Mogi *et al.* [61] and Tu *et al.* [58].

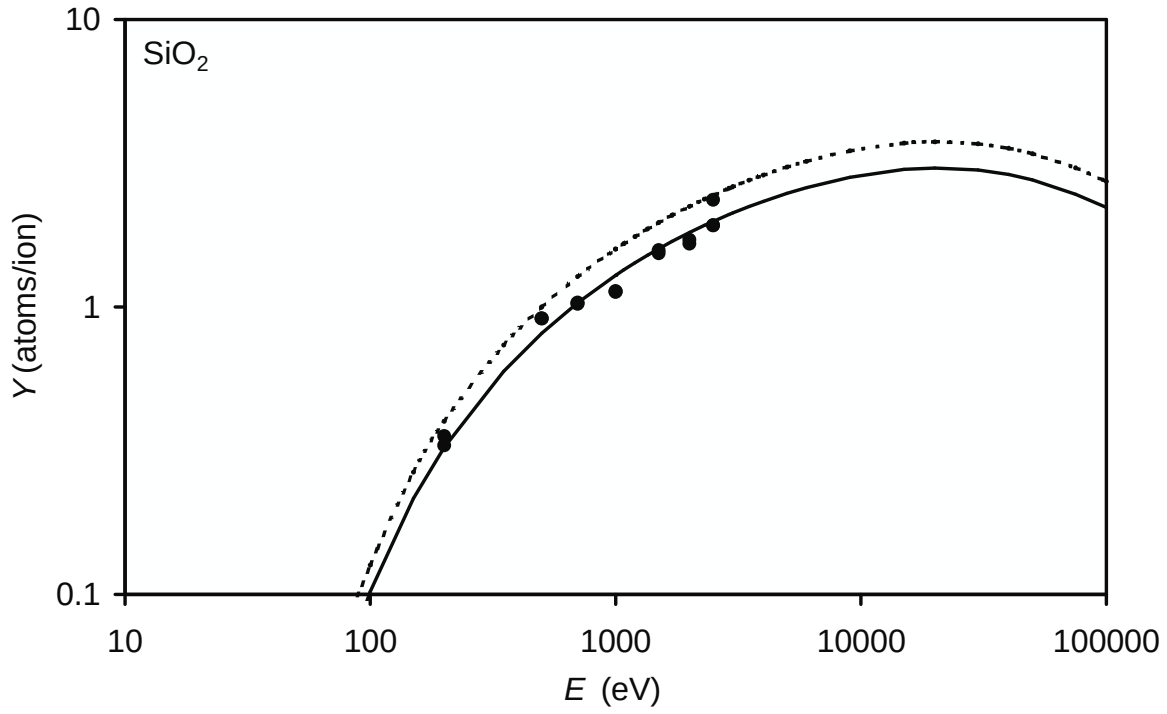

Figure 10. The sputtering yield $Y(\infty)$ for SiO_2 using argon ions at normal incidence. The dashed curve is the result for the semiempirical equation with interpolated parameters, and the solid curve is that result scaled by 0.81.

In preliminary tests with a different instrument and system and with higher ion beam current densities, crater shapes were found that were not of the shape expected. This was attributed to the effects of sample charging. The thermal oxide on Si is, of course, an insulator and so charging is expected. In those preliminary tests, it was concluded that the craters either exhibited beam deflection or material re-deposition leading to significantly reduced apparent yields.

The Thermo Scientific K-Alpha system used here has an electron flood, charge neutralisation system and its effectiveness is shown by the excellent stability of the XPS peak energies. It is likely, therefore, that unlike the other materials systems discussed here, SiO_2 can charge if adequate neutralization is not available, leading to the scatter of data and generally lower yields. It is difficult, therefore, to recommend SiO_2 as a very general depth profiling standard since it is unclear how much a given level of charging, if charging is the correct explanation, affects the measured yield. Of course, individual laboratories that have developed relevant expertise, can obtain excellent results with SiO_2 but interlaboratory comparability is still poor.

It is clear that the energy dependencies of the sputtering yields of compounds may be calculated accurately but that the experimental data lie within upper and lower bounds set by ignoring and including H_{AB} such that the greater the value of H_{AB}, the greater the absolute uncertainty. An illustration of the value of accurately defining the energy dependence is shown from the data of Mogi *et al.* [61] reporting an extensive and careful study of the relative sputtering rates (nm/s) of SiO_2 and Si in many laboratories using argon ions at 1 and 3 keV beam energies. The data and predictions are shown in figure 11 where error bars have been added based on the standard uncertainties of the means of the experimental data expanded by a factor of 2 for a confidence level of 95% in the means. The match between the data and calculations is excellent and supports the present approach. Note that the ordinate is around unity not through normalization but as a ratio of absolute sputtering rates.

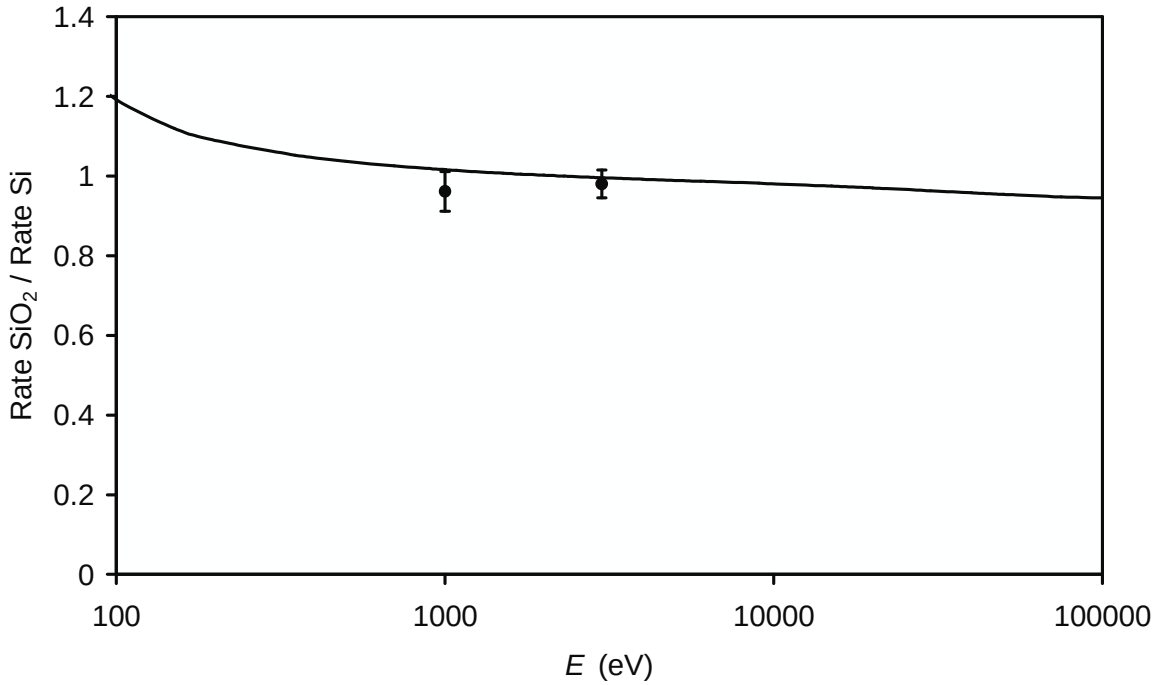

Figure 11. The ratio of the sputtering rates in nm/s for SiO_2 and Si as a function of the argon sputtering energy at normal incidence. The curve is calculated from $Y(\infty)$ for SiO_2 from the semiempirical theory scaled by 0.81 as found by experiment and from Y for Si calculated as described previously. The data are from Mogi *et al.* [61] with uncertainties taken from their standard deviations, divided by the square root of the number of results and expanded by a factor of 2 for a confidence level of 95%.

7. Conclusions

In the prediction of equilibrium sputtering yields for compounds, fundamental theories need to incorporate the implantation and out-diffusion of the primary ion species, preferential sputtering, the changes of density and bond energies with composition, and the depth and energy dependence of these effects in addition to the customary properties of the sample. Some of these effects serve to raise, and others to lower, the sputtering yield to extents that are difficult to calculate. By analysing the data for one material with close atomic numbers and weak preferential sputtering (GaAs) and one with widely separated atomic numbers and strong preferential sputtering (Ta_2O_5), it is shown that the semi-empirical theory of Seah [3,4] gives excellent results for the equilibrium sputtering yield when the preferential sputtering is ignored. This is justified in terms of the simple pair-bonding theory often used in layer-by-layer studies. Similar calculations using SRIM 2006 show good results when the input parameters discussed here are used instead of the default parameters, although the correlations with experimental data, although good, are significantly poorer than for the semi-empirical theory.

Analysis of a wide range of oxide sputtering data show that the heat of reaction or mixing, H_{AB}, needs to be incorporated in the binding energy term, U_o. If H_{AB} is ignored, the experimental data are lower than the predictions, typically by a factor of 0.68. The effect of H_{AB} is easy to include but, if the preferential sputtering, atomic mixing, etc. are strong, the effect of H_{AB} in the outermost layer is diminished and its effect reduced. This is confirmed using published measurements of the preferential sputtering. With this effect included, the experimental data are, on average, equal to the predictions but with a standard uncertainty of 16%. In this way, through a different route, the preferential sputtering is important. For SiO_2, often used as a sputtering reference material, existing data are very scattered (a scatter factor of 1.5). New data show excellent consistency with the above semi-empirical model (9%) when using interpolated parameters. These data indicate that charging may have been a problem with some of the historical sputtering yield data for SiO_2. The calculation of the absolute yields of oxides, using equations (1) to (13) with interpolation, coupled with U_{int} replaced by $U_{int} + xH_{AB}$, where x is evaluated from the preferential sputtering, has a standard uncertainty of 16% but the energy dependencies appears to be an effective procedure.

Acknowledgements

The author would like to thank Steve Spencer for calculations using MTDATA and for the mapping ellipsometry of the SiO_2 crater, Joanna Lee for preliminary sputtering trials in a SIMS instrument, Jim Ziegler and Johan Malherbe for helpful comments. This work is supported by the National Measurement System of the UK Department for Innovation, Universities and Skills through the Chemical and Biological Metrology Programme.

References

[1] Hofmann S 1990 *Practical Surface Analysis, Second Edn, Volume 1, Auger and X-ray Photoelectron Spectroscopy* eds D. Briggs and M. P. Seah (Chichester: Wiley) p 143-199

[2] Wagner T, Wang J Y and Hofmann S 2003 *Surface Analysis by Auger and X-ray Photoelectron Spectroscopy* eds D. Briggs and J. T. Grant (Chichester: I M Publications and Surface Spectra) Chapter 22, p 619-649

[3] Seah M P, Clifford C A, Green F M and Gilmore I S 2005 *Surf. Interface Anal*. **37** 444-458

[4] Seah M P 2005 *Nucl. Instrum. Methods B* **229** 348-358

[5] Seah M P 2005 *Nucl. Instrum. Methods B* **239** 286-287

[6] Matsunami N, Yamamura Y, Hikawa Y, Itoh N, Kazumata Y, Miyagawa S, Morita K, Shimizu R and Tawara H 1984 *At. Data Nucl. Data Tables* **31** 1-80

[7] Sigmund P 1969 *Phys. Rev*. **184** 383-416

[8] Yamamura Y, Itakawa Y and Itoh N 1983 *Institute of Plasma Physics Report IPPJ-AM-26*, (Nagoya: University Press)

[9] Zimmermann S and Urbassek H M 2008 *Int. J. Mass Spectrom*. **272** 91-97

[10] Szymczak W and Wittmaack K 1993 *Nucl. Insrum. Meths. B* **82** 220-233

[11] Seah M P 2007 *Surf. Interface Anal*. **39** 634-643

[12] Sigmund P and Claussen C J 1981 *Appl. Phys*. **52** 990-993

[13] Bouneau S, Brunelle A, Della Negra S, Depauw J, Jacquet D, Le Beyec Y, Pautrat M, Fallavier M, Poizat J C and Andersen H H 2002 *Phys. Rev. B* **65** 144106

[14] Samela J, Kotakoski J, Nordlung K and Keinonen J 2005 *Nucl. Instum. Meths B* **239** 331-346.

[15] Seah M P, Spencer S J, Cumpson P J and Johnstone J E 2000 *Surf. Interface Anal.* **29** 782-790

[16] Lindhard J, Scharff M and Schiott H E 1963 *Mat. Fys. Medd. Dan. Vid. Selsk*. **33** (14) 1-42

[17] Matsunami N, Yamamura Y, Itakawa Y, Itoh N, Kazumata Y, Miyagawa S, Morita K and Shimizu R 1980 *Radiat. Eff. Lett*. **57** 15-21

[18] Bragg W H and Kleeman R 1905 *Philos. Mag.* **10** 318-340

[19] Sigmund P 1981 *Topics in Applied Physics 47: Sputtering by Particle Bombardment I* ed R Behrisch (Berlin: Springer) p 9-71

[20] Malherbe J B 1994 *Crit. Revs. in Solid State Mater. Sci*. **19** 55-127

[21] Ziegler J F and Manoyan J M 1988 *Nucl. Instrum. Methods, B* **35** 215-228

[22] Kelly R 1985 *Surf. Interface Anal.* **7** 1-7

[23] Betz G and Wehner G K 1983 *Topics in Applied Physics 52: Sputtering by Particle Bombardment II* ed R. Behrisch (Berlin: Springer) p 11-90

[24] Malherbe J B 1994 *Crit. Revs. in Solid State Mater. Sci*. **19** 129-195

[25] Malherbe J B and Odendaal R Q 1998 *Surf. Interface Anal*. **26** 841-850

[26] Anders C and Urbassek H M 2005 *Nucl. Instrum. Methods B* **228** 84-91

[27] Kelly R and Lam N Q 1973 *Radiation Effects* **19** 39-47

[28] Kelly, R 1980 *Surf. Sci.* **100** 85-107

[29] Kelly R and Harrison D E 1985 *Mat. Sci. Eng*. **69** 449-455

[30] Seah M P, Green F M and Gilmore I S 2010 *J. Am. Soc. Mass Spectrom* **21** 370-377

[31] *MTDATA – Thermodynamics and Phase Equilibrium Software*, (Teddington: National Physical Laboratory) http://www.npl.co.uk/mtdata/

[32] Kubaschewski O and Alcock C B 1979 *Metallurgical Thermochemistry*, 5th Edn. (Oxford: Pergamon)

[33] *Center for Research in Computational Thermochemistry*, at http://www.crct.polymtl.ca

[34] Smithels C J 1976 *Metals Reference Book*, 5th edn. (London: Butterworths)

[35] *SRIM 2006* available free from www.srim.org/SRIM/SRIM2006.htm

[36] Hunt C P and Seah M P 1983 *Surf. Interface Anal.* **5** 199-209

[37] *BCR 261T* available from IRMM. See http://www.irmm.jre.be/html/homepage.htm

[38] Steffen J and Hofmann S 1988 *Surf. Interface Anal.* **11** 617-626

[39] Hofmann S and Steffen J 1989 *Surf. Interface Anal*. **14** 59-65

[40] Steffen J and Hofmann S 1989 *Fres. Z. Anal. Chem*. **333** 408-409

[41] Hofmann S and Sanz J M 1982-3 *J. Trace and Microprobe Techniques*. **1** 213-264

[42] Tapping R L, Davidson R D and Jackman T E 1985 *Surf. Interface Anal.* **7** 105-108

[43] Tapping R L, Davidson R D, Jackman T E and Davies J A 1988 *Surf. Interface Anal*. **11** 441-446
[44] Wild R K 1989 *Surf. Interface Anal*. **14** 239-244
[45] Viefhaus H, Hennesen K, Lucas M, Müller-Lorenz E M and Grabke H J 1994 *Surf. Interface Anal*. **21** 665-672
[46] Engelhard M H, Baer D R, Lea A S, Droubay T C, Kuchibhalla S V, Matthews C S, Lee B, Kim J, Wallace R M and Stickle W F 2009 private commun.
[47] Malherbe J B, Hofmann S and Sanz J M 1986 *Appl. Surf. Sci*. **27** 355-365
[48] Hines R L 1957 *J. Appl. Phys*. **28** 587-591
[49] Jorgenson G V and Wehner G K 1965 *J. Appl. Phys.* **36** 2672-2674
[50] Dugdale R A and Ford S D 1966 *Trans. Br. Ceram. Soc.* **65** 165-180
[51] Davidse P D and Maissel L I 1967 *J. Vac. Sci. Technolog*. **4** 33-36
[52] Bach H 1970 *Nucl. Instrum. Meths*. **84** 4-12
[53] Tarasevich M 1970 *Appl. Opt*. **9** 173-176
[54] Bayly A R 1972 *J. Mater. Sci*. **7** 404-412
[55] Cantarel M and Marchal M 1973 *J. Mater. Sci*. **8** 1711-1716
[56] Edwin R P 1973 *J. Phys. D* **6** 833-841
[57] Bach H, Klitzmann I and Schröder H 1974 *Rad. Effects* **21** 31-36
[58] Tu Y Y, Chuang T J and Winters H F 1981 *Phys. Rev. B* **23** 823-835
[59] Bach H 1988 *J. Non Crystalline Solids* **102** 36-42
[60] Nenadović T, Perraillon B, Bogdanov Z, Djordjević Ž and Milić M 1990 *Nucl. Instrum. Meths. B* **48** 538-543
[61] Mogi K, Ogiwara T and Suzuki M 2002 *J. Surf. Anal*. **9** 514-523
[62] Smentkowski V S 2000 *Progr. in Surf. Sci*. **64** 1-58
[63] Veisfeld N and Geller J D 1988 *J. Vac. Sci. Technol. A* **6** 2077-2081
[64] Seah M P, Spencer S J, Bensebaa F, Vickridge I, Danzebrink H, Krumrey M, Gross T, Oesterle W, Wendler E, Rheinländer B, Azuma Y, Kojima I, Suzuki N, Suzuki M, Tanuma S, Moon D W, Lee H J, Hyun Mo Cho, Chen H Y, Wee A T S, Osipowicz T, Pan J S, Jordaan W A, Hauert R, Klotz U, van der Marel C, Verheijen M, Tamminga Y, Jeynes C, Bailey P, Biswas S, Falke U, Nguyen N V, Chandler-Horowitz D, Ehrstein J R, Muller D and Dura J A 2004 *Surf. Interface Anal*. **36** 1269-1303
[65] Homma Y, Takenaka H, Toujou F, Takano A, Hayashi S and Shimizu R 2003 *Surf. Interface Anal.* **35** 544-547
[66] Johannessen J S, Spicer W E and Strausser Y E 1976 *J. Appl. Phys*. **47** 3028-3037
[67] Yakabe T, Fujita D and Yoshihara K 2005 *Appl. Surf. Sci*. **241** 127-130
[68] Seah M P, Unger W E S, Hai Wang, Jordaan W, Gross Th, Dura J A, Moon D W, Totarong P, Krumrey M, Hauert R and Mo Zhiqiang 2009 *Surf. Interface Anal.* **41** 430-439